

Three oxidation states and atomic-scale p – n junctions in manganese perovskite oxide from hydrothermal systems

Shouhua Feng · Hongming Yuan · Zhan Shi · Yan Chen ·
Yongwei Wang · Keke Huang · Changmin Hou ·
Jixue Li · Guangsheng Pang · Ying Hou

Received: 5 November 2006 / Accepted: 11 July 2007 / Published online: 22 December 2007
© Springer Science+Business Media, LLC 2007

Abstract Perovskite oxides have provided magical structural models for superconducting and colossal magnetoresistance, and the search for nano-scale and/or atomic-scale devices with particular property by specific preparations in the same systems has been extensively conducted. We present here the three oxidation states of manganese (Mn^{3+} , Mn^{4+} , Mn^{5+}) in the perovskite oxide, $\text{La}_{0.66}\text{Ca}_{0.29}\text{K}_{0.05}\text{MnO}_3$, which most interestingly shows the rectifying effect as atomic-scale p – n junctions (namely FY-Junctions) of single crystals and films. The family of cubic perovskite oxides were synthesised by the so-called hydrothermal disproportionation reaction of MnO_2 under the condition of strong alkali media. The new concept of the atomic-scale p – n junctions, based on the ideal rectification characteristic of the p – n junctions in the single crystal, basically originates from the structural linkages of $[\text{Mn}^{3+}\text{O}-\text{Mn}^{4+}\text{O}-\text{Mn}^{5+}]$, where Mn^{3+} ($t_{2g}^3 e_g^1$) and Mn^{5+} ($t_{2g}^2 e_g^0$) in octahedral symmetry serve as a donor and an acceptor, respectively, corresponding to the localized Mn^{4+} ($t_{2g}^3 e_g^0$).

Introduction

Perovskite oxides with a general formula ABO_3 ($A = 12$ -coordinated ions and $B = 6$ -coordinated ions) provide magical structural models for superconducting and colossal

magnetoresistance [1–3]. Among the most interesting issue has been the creation of complicated mixed valence states, which implies further new models with particular electron–electron and electron–lattice interactions [4, 5]. Two oxidation states of manganese are common in alkaline-earth metal-doped lanthanum manganite perovskites and show colossal magnetoresistance (CMR) by the double-exchange (DE) mechanism [6, 7]. Finding more complicated oxidation states of manganese in the perovskites is a great challenge in the search for new materials with nano-scale and/or atomic-scale functions through specific preparations. High-temperature solid state reactions [8], charge disproportionation [9, 10] and fluctuation [11] have been considered to be useful, but these preparative methods only led to two oxidation states. Hydrothermal synthesis has been successfully applied to the most important crystalline materials, advantageous to perfect crystals and stabilizing unusual oxidation states [12]. Our motivation for creating complicated mixed valence of metal in perovskite system comes from the consideration that complicated mixed valence such as three oxidation states of a metal may provide some kind of “junction” property in an atomic-scale compared to a macro-scale p – n junction commonly consisting of $[\text{P}]-[\text{Si}]-[\text{Ga}]$, rather than the DE property occurred between two oxidation states. We understand that single electron system is also an important factor for preparing a strong electron correlation solid; in our selected system the single e_g electron on 3d orbital of Mn in octahedral environment of perovskite oxide may play an important role in forming such a “junction”. In the preparation of complicated mixed valence compounds, hydrothermal solution may serve such a place where redox or disproportionation reaction may produce ions with at least three oxidation states, and the following steps should be how to stabilize and crystallize them into a solid.

S. Feng (✉) · H. Yuan · Z. Shi · Y. Chen · Y. Wang ·
K. Huang · C. Hou · J. Li · G. Pang · Y. Hou
State Key Laboratory of Inorganic Synthesis & Preparative
Chemistry, College of Chemistry, Jilin University, Changchun
130012, P.R. China
e-mail: shfeng@mail.jlu.edu.cn

Experimental

The synthesis of our sample involves a hydrothermal disproportionation reaction of MnO_2 at 260 °C for 2–3 days. The initial materials were $\text{La}(\text{NO}_3)_3 \cdot 6\text{H}_2\text{O}$, MnO_2 , $\text{Ca}(\text{NO}_3)_2 \cdot 4\text{H}_2\text{O}$, and KOH . Commercial agent MnO_2 or freshly prepared MnO_2 was used in the synthesis. The prepared MnO_2 was produced by the reduction of an aqueous solution of KMnO_4 with fumaric acid ($\text{HO}_2\text{CCH}=\text{CHCO}_2\text{H}$) [13]. The synthesis of MnO_2 was performed in 500 mL beaker. About 30 g KOH was added into 260 mL 0.12 M KMnO_4 to form an alkaline solution, into which 3.62 g fumaric acid was added with stirring. The obtained dark brown gel was filtered and dried at 50 °C for 24 h prior to use. In a typical hydrothermal synthetic procedure for our sample 1.4 g so-obtained MnO_2 were added into 40 mL water to form a solution on stirring, to which 20 mL 0.4 M $\text{La}(\text{NO}_3)_3$, 5 mL 0.4 M $\text{Ca}(\text{NO}_3)_3$, and 65 g KOH were in turn added. The reaction mixture was stirred with a magnetic stirrer for 30 min and then transferred into an 80 mL teflon-lined stainless steel autoclave with a filling capacity of 80%. The crystallization was carried out under autogenous pressure at 260 °C for 3 days. After the autoclave was cooled and depressurized, the powder products were washed thoroughly with distilled water and sonicated by a direct immersion titanium horn (Vibracell, 20 kHz, 200 w/cm²). The dark-green crystals were obtained. Inductively coupled plasma (ICP) analysis was performed on a Perkin-Elmer Optima 3300DV ICP instrument. HRTEM observations were conducted with a PHILIPS CM200 field-emission transmission electron microscope operated at 200 kV and room temperature. SEM was carried out on a field-emission JSM-6700F JEOL microscope. The near IR absorption measurement was performed using the UV-3100 Shimadzu ultraviolet-visible-infrared spectrophotometer. The spectra of Mn *K*-edge XANES were measured at the beamline of 1W1B of Beijing Synchrotron Radiation Facility (BSRF). The storage ring was operated at 2.2 GeV with a typical current of 100 mA. The fixed-exit Si(111) flat double crystals were used as monochromator. The spectra were recorded in transmission mode with ionization chambers filled with nitrogen. The NIR emission spectra were recorded at room temperature on an Acton SpectroPro 2758 spectrograph with InGaAs NIR detector. A spectra-Physics Quanta-Ray Nd: YAG was used as excitation source (1,064 nm). The work function measurement was carried out on a commercial Kelvin Probe (KP Technology Ltd., England) at room temperature in atmosphere. The Kelvin probe is vibrating capacitor device for measuring the work function difference between the simple and vibrating tip (gold tip with a work function of 5.1 eV is used in this work). The sample powders were spread horizontally on polished Al substrate. In the CITS

test, Gold (99.99%) was thermally evaporated onto the freshly cleaved silicon wafer at a pressure of 5×10^{-5} Pa to make a gold film. Single crystals were spread on the gold film of AFM sample holder. The load force of the gold tip was maintained at 2 Nm^{-1} . A bias voltage between the substrate (gold film) and the gold tip of the conducting cantilever for I–V measurements was scanned from –10 to +10 V. Each time we conducted this experiment, we tested the connection of the gold tip to the gold substrate (\sim zero voltage) and to an insulator (\sim zero current). Before and after each experiment the electrical conductivity between the cantilever and gold film was verified by measuring the tip current in order to monitor the possibility of whether the tip had been broken during the scanning process.

Results and discussion

Hydrothermal disproportionation

Our study began with the synthesis of CMR manganese perovskite oxides, and a cubic phase of $\text{La}_{0.5}\text{Ba}_{0.5}\text{MnO}_3$ was synthesised under mild hydrothermal conditions [14]. With an aim towards stabilizing particularly mixed valences of metal in crystals, we carried out the hydrothermal synthesis of normal manganese perovskite oxides through the disproportionation reactions of MnO_2 . In this study we obtained a family of manganese perovskite oxides, $\text{La}_{1-x-y}\text{Ca}_x\text{K}_y\text{MnO}_3$ ($x = 0.74\text{--}0.18$, $y = 0.01\text{--}0.14$) through the partial substitution of Ca^{2+} and K^+ for La^{3+} under the condition of strong alkali media. Single crystal X-ray diffraction (XRD) structural analysis for one member of the family, $\text{La}_{0.66}\text{Ca}_{0.29}\text{K}_{0.05}\text{MnO}_3$, compositionally analysed by inductively coupled plasma (ICP), indicated its cubic perovskite structure [15]. The scanning electronic microscopic (SEM) photos and the crystal structure for $\text{La}_{0.66}\text{Ca}_{0.29}\text{K}_{0.05}\text{MnO}_3$ are shown in Figs. 1 and 2. Since the single crystal X-ray diffraction determination did not distinguish the types of A-site atoms, we need to probe if the composition of our single crystal sample consists with the ICP analysis for elements of La, Ca and K. The high-resolution transmission electron microscopy (HRTEM) image (Fig. 3) firstly confirmed the cubic structure, and then the energy dispersive X-ray spectroscopy (EDX) on-line analysis on the same area clearly detected the existence and ratio of O, K, La, Ca, and Mn elements in the lattice (Fig. 4). In addition, the element mapping illustrated the uniform composition in the single crystals (Fig. 5).

Three oxidation states

Mn average oxidation state in $\text{La}_{0.66}\text{Ca}_{0.29}\text{K}_{0.05}\text{MnO}_3$ was firstly measured by means of oxidation–reduction titration

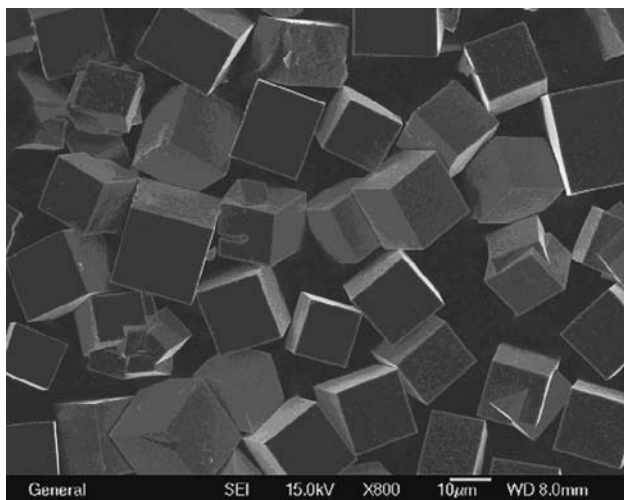


Fig. 1 SEM photo of $\text{La}_{0.66}\text{Ca}_{0.29}\text{K}_{0.05}\text{MnO}_3$ crystal samples

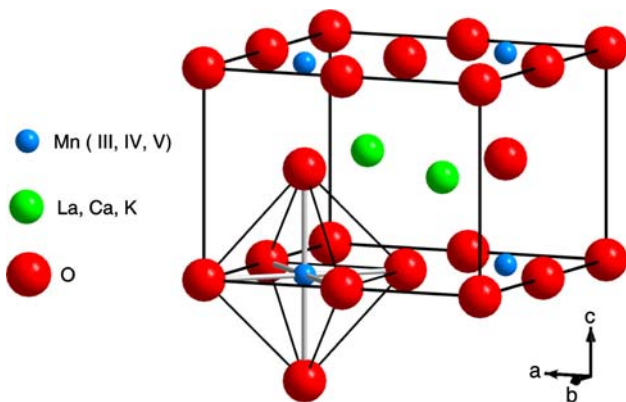


Fig. 2 Single crystal structure of $\text{La}_{0.66}\text{Ca}_{0.29}\text{K}_{0.05}\text{MnO}_3$

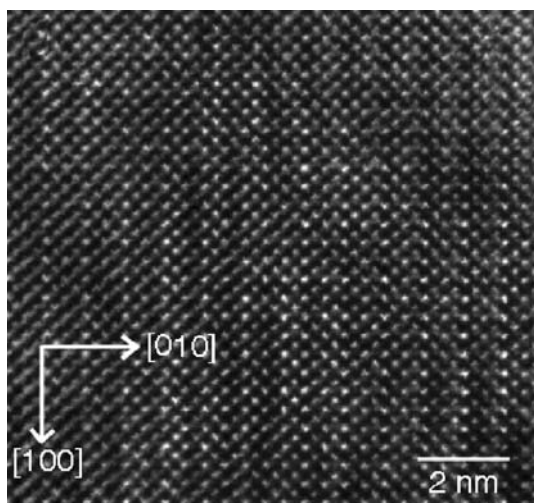


Fig. 3 HR-TEM image of $\text{La}_{0.66}\text{Ca}_{0.29}\text{K}_{0.05}\text{MnO}_3$

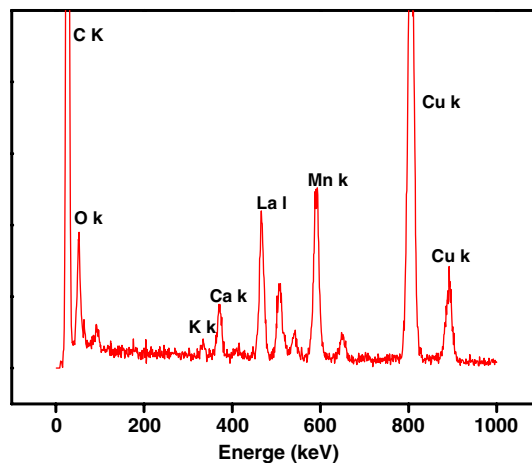


Fig. 4 HR-TEM-EDX compositional analysis of $\text{La}_{0.66}\text{Ca}_{0.29}\text{K}_{0.05}\text{MnO}_3$

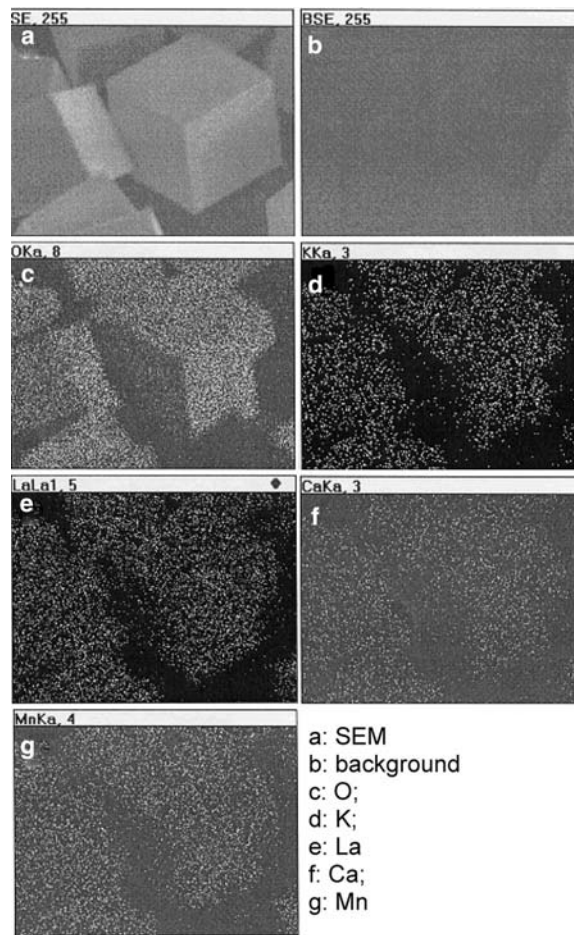


Fig. 5 SEM-EDX map of $\text{La}_{0.66}\text{Ca}_{0.29}\text{K}_{0.05}\text{MnO}_3$

(Iodometry). The experimental average valence of 3.36 is much close to its theoretical value of 3.38, which is calculated by charge balance in A- (La^{3+} , Ca^{2+} , K^+) and B-site ions (Mn^{3+} , Mn^{4+} , Mn^{5+}) according to Dalton law. The

important issue of oxygen defect in our sample was considered at the very beginning of this study. Thermal analyses showed no thermal effect as well as weight loss at temperature measured up to 1,200 °C, which is very much consistent with the normal sense, e.g., hydrothermal system gives equilibrium defect of crystal as in the case of quartz hydrothermal production. The identification of Mn^{5+} in our sample was made by its characteristic near infrared (IR) absorption at 625 nm due to the ${}^3\text{T}_1(\text{t}_2^2) \rightarrow {}^1\text{A}_1(\text{t}_2^2)$ excitation according to Noginov et al. [16] (Fig. 6). Mn K-edge X-ray absorption near-edge spectroscopic (XANES) spectra for $\text{La}_{0.66}\text{Ca}_{0.29}\text{K}_{0.05}\text{MnO}_3$, different from the known manganese perovskite oxides [17], evidenced an additional peak centred at 6564.3 eV, the energy of the band edge of 1s to 4p transitions for Mn^{5+} (Fig. 7). The same peak at ca 6565 eV was found in the K-edge XANES spectrum of the synthetic apatite, $\text{Ba}_5(\text{PO}_4)_2.5(\text{MnO}_4)_{0.5}\text{Cl}$, where all of the Mn ions have +5 oxidation state, and it has been taken as a reference of Mn^{5+} in tetrahedral coordination [18]. In our case, a slight decrease in the K-edge absorption energy is expected since the octahedral Mn^{5+} has less effectively positive charges than the tetrahedral Mn^{5+} . An additional evidence showing the existence of Mn^{5+} is the laser-induced (1,064 nm) luminescence spectroscopy for our sample compared with the mineral sample $\text{K}_{0.1}\text{Sr}_{0.9}\text{MnO}_3$, where all of the Mn ions are in +5 oxidation state. The typical emissions at 1,143, 1,169, and 1,224 nm for Mn^{5+} ion in $\text{K}_{0.1}\text{Sr}_{0.9}\text{MnO}_3$ were also found in our sample (Fig. 8) [19], whereas the $\text{Mn}^{3+}\text{--Mn}^{4+}$ sample we made before showed no emissions at the above three wavelengths. The formation of the three mixed valence of $\text{Mn}^{3+}\text{--Mn}^{4+}\text{--Mn}^{5+}$ in the perovskite oxide is thermodynamically allowed based on the hydrothermal disproportionation reaction, $2\text{Mn}^{\text{IV}}\text{O}_2 + 2\text{OH}^- = \text{Mn}^{\text{III}}\text{O}_3^{3-} + \text{Mn}^{\text{V}}\text{O}_3^- + \text{H}_2\text{O}$, where

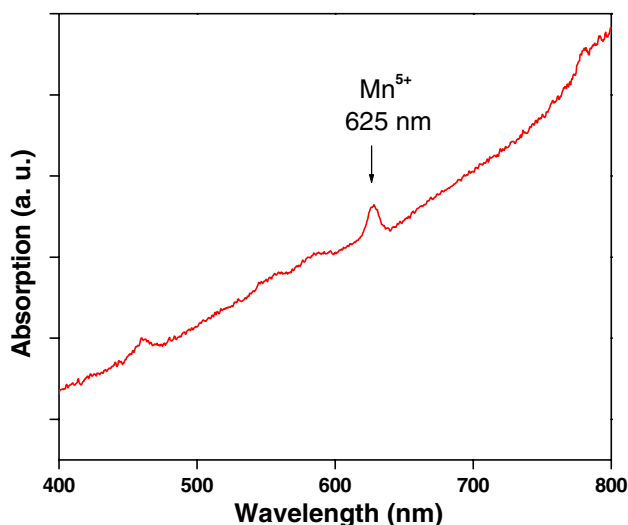


Fig. 6 Near IR spectrum of $\text{La}_{0.66}\text{Ca}_{0.29}\text{K}_{0.05}\text{MnO}_3$

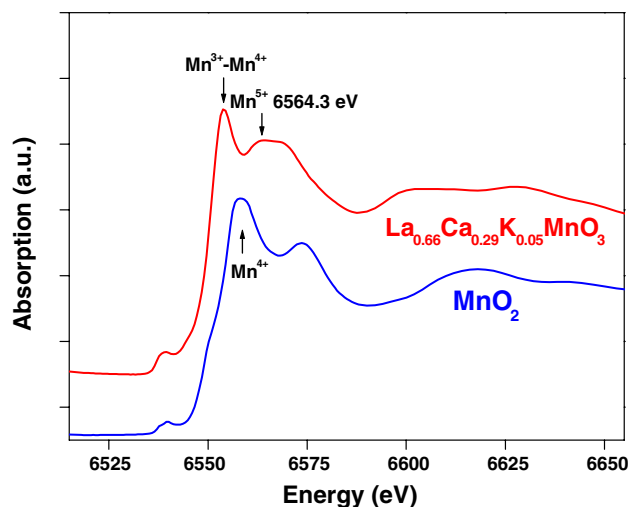


Fig. 7 Mn K-edge XANES spectra of $\text{La}_{0.66}\text{Ca}_{0.29}\text{K}_{0.05}\text{MnO}_3$ and reference MnO_2

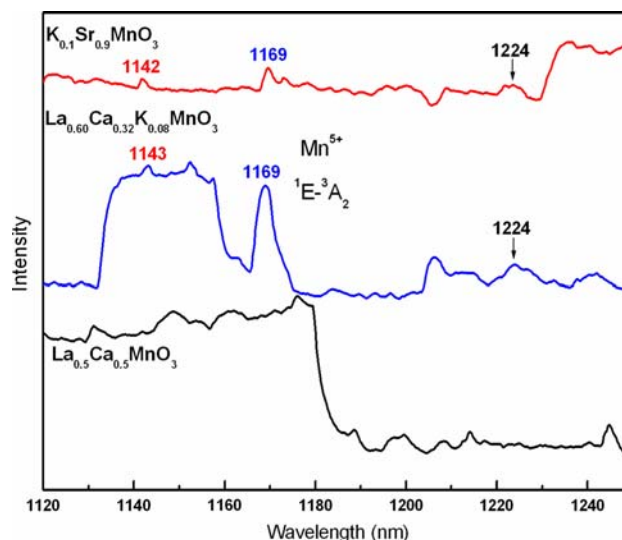


Fig. 8 Laser-induced luminescence spectra of $\text{K}_{0.1}\text{Sr}_{0.9}\text{MnO}_3$, $\text{La}_{0.66}\text{Ca}_{0.29}\text{K}_{0.05}\text{MnO}_3$, and $\text{La}_{0.5}\text{Ca}_{0.5}\text{MnO}_3$

MnO_2 itself was dissolved in solution first, $\text{Mn}^{\text{IV}}\text{O}_2 + 2\text{OH}^- = \text{Mn}^{\text{IV}}\text{O}_3^{2-} + \text{H}_2\text{O}$.

In fact, the intermediates of Mn^{3+} , Mn^{4+} , Mn^{5+} , and Mn^{6+} in solution were detected, and interestingly Mn^{5+} was formed at the early stage of the oxidation–reduction reactions of MnO_4^- with carboxymethyl cellulose polysaccharide at $\text{pH} > 12$ [20]. These intermediates were considered to be short-lived, but could be stabilized in solids, such as in Mn^{5+} -based solid state lasers [21] and satirically rigid olefins [22]. The single crystal of the perovskite $\text{Ba}_{1+x}\text{Na}_x\text{Mn}_{1-x}\text{O}_3$ with 1:1 of Mn^{4+} and Mn^{5+} was prepared by electro-synthesis in molten NaOH [23]. In our specific hydrothermal synthesis, the strong alkaline

media created the possibility of the occurrence of the disproportionation reaction and the formation of multivalent Mn ions as well. The stabilization of three oxidation state Mn ions into solid states further enhanced the reaction. Structurally, the charges of the three oxidation state Mn ions at B-sites were compensated by their three corresponding A-site ions of La^{3+} , Ca^{2+} and K^{+} to maintain the charge neutrality in the perovskite oxide.

Atomic-scale *p-n* junctions

We have been very interested in revealing experimentally the nature of the three oxidation states of manganese in the perovskite oxides. Apparently, the current-voltage (*I-V*) measurements on single crystal may give accurate information; we thus measured *I-V* curves on our single crystals by conductive atomic force microscopy (C-AFM), which is useful in detecting the electrical properties of small sized crystals (in our case 20–40 μm “cubic” crystals) by the well-established point-contact modes [24–27]. To ensure the ohmic contact of the gold tip (*ca* 5 nm in diameter) with the single crystal surface, we tested the work function of our sample (4.9 eV), which is very close to that of the reference gold (5.1 eV). Figure 9 shows the three-dimensional plot of work function for our sample. We repeatedly measured *I-V* curves on more than thousand single crystals and statistically found two types of *I-V* curves as shown in Fig. 10. Clearly, the ideal rectifying characteristics of *p-n* junctions as tunnel diodes were devised by the *I-V* measurements on the single crystals. These ideal *I-V* characteristics of *p-n* junctions found in our single crystals illustrate the nature of the atomic-scale *p-n* junctions. They are almost the same as the *I-V* characteristics of the

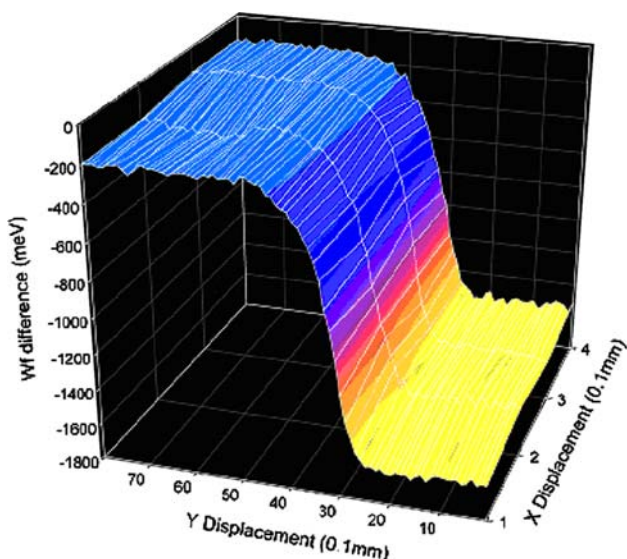


Fig. 9 Three-dimensional plot of the work function for the sample

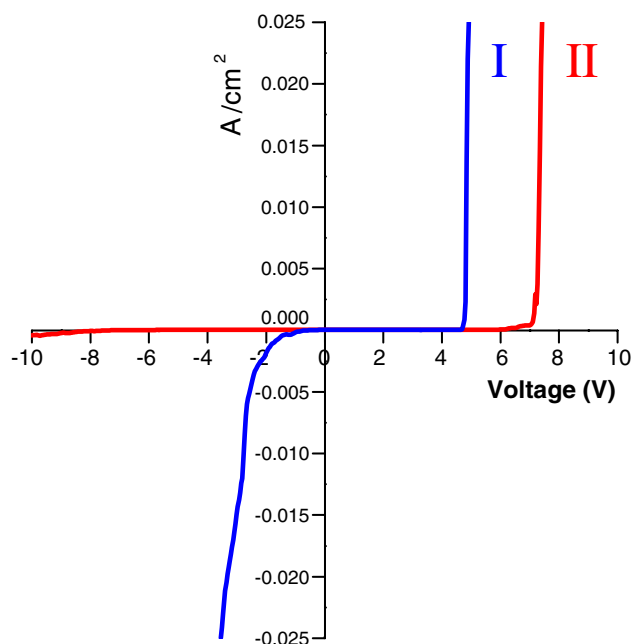


Fig. 10 *I-V* characteristics of the atomic-scale *p-n* junctions for single crystals

molecular rectifier theoretically calculated by Aviram and Ratner [28]. Experimentally, we do distinguish clearly the compositional controlled structures as the HR-TEM image shown in Fig. 11, which may be correlated to the anisotropic electrical properties in the *I-V* measurements. Although we have the cubic structure, this image shows clearly the double layers along the (010) direction. Possibly, these two types of *I-V* curves may have resulted from the super-lattice structures, but this needs further study. All

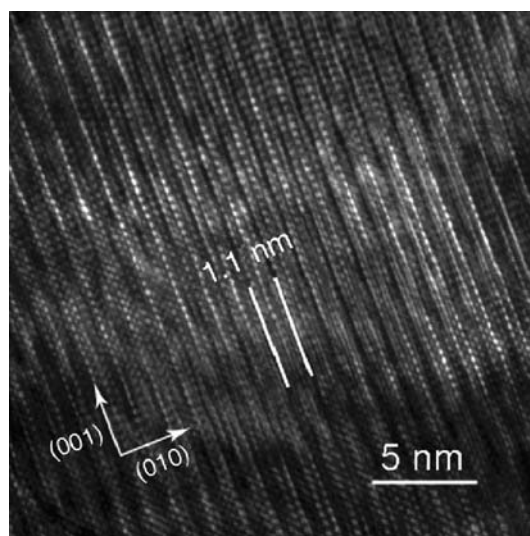


Fig. 11 HR-TEM image for a super-lattice sample of $\text{La}_{0.66}\text{Ca}_{0.29}\text{K}_{0.05}\text{MnO}_3$

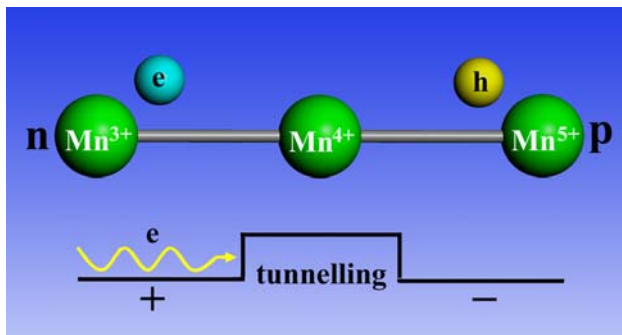


Fig. 12 Schematic array for an atomic-scale p - n junction consisting of $\text{Mn}^{3+}\text{-O-Mn}^{4+}\text{-O-Mn}^{5+}$ in (110) or (001) directions. Oxygen atoms were omitted for clarity. The symbols e and h represent electron and hole, respectively

of the phenomena, reflected from the single crystal structure and its I-V measurement, lead to the conclusion of the existence of the atomic-scale p - n junctions in our crystal. In addition, our materials show high thermal stability, giving the same I-V curves after treatment at 1,200 °C for 10 h, implying possible high-temperature applications.

Figure 12 illustrates the model for the proposed atomic-scale p - n junction. In the three mixed valence perovskite oxide, the structural linkages such as $\text{Mn}^{3+}\text{-O-Mn}^{4+}$, and $\text{Mn}^{3+}\text{-O-Mn}^{4+}\text{-O-Mn}^{5+}$ (the linkage of $\text{Mn}^{3+}\text{-O-Mn}^{5+}$ is hardly considered, because at high temperature the disproportionation reaction may take place) are expected according to its structure and composition. The most possible array of $\text{Mn}^{3+}\text{-O-Mn}^{4+}\text{-O-Mn}^{5+}$ gives rise to the construction of an atomic-scale p - n junction, similar to a macroscopic p - n junction in a semiconductor. In the atomic-scale p - n junction, Mn^{3+} ($t_{2g}^3 e_g^1$) and Mn^{5+} ($t_{2g}^2 e_g^0$) in the octahedral site symmetry may serve as a donor and an acceptor, respectively through the localized Mn^{4+} ($t_{2g}^3 e_g^0$). A built-in field may be set up by e_g electron tunnelling from Mn^{3+} ($t_{2g}^3 e_g^1$, donor) to Mn^{5+} ($t_{2g}^2 e_g^0$, acceptor) over an energy barrier. The above I-V measurements on the single crystals strongly support the arrangement of the atomic-scale p - n junctions. When a forward bias is applied to a p - n junction, the potential barrier is reduced if the p -side is made positive. It is fairly obvious qualitatively that the number of electrons flowing from p -side to n -side is not affected in either case, but the flow of electrons from n -side to p -side is seriously affected. So we can see qualitatively that the total current flowing for a positive voltage will differ from the current flowing at a negative voltage. Our model may provide the basis for further theoretical study on the atomic-scale p - n junctions.

Conventionally it is possible to turn a crystal such as pure silicon into a moderately good semiconductor by adding impurity phosphorus for an n -type semiconductor or gallium for a p -type semiconductor. Useful applications

start to happen only when a single semiconductor crystal contains both n -type and p -type regions, consisting of a macroscopic p - n junction. Moreover, since the silicon with a bandgap of 1.12 eV can effectively use only the wavelengths in the range of ca 0.4–1.1 μm , more complex photovoltaic devices with multi-junctions can use more of the spectrum and should be operated at high efficiencies than the single-junction devices. In our case, as the junctions may be connected in three dimensions, the switching voltage of each junction must match; hence the device switching voltage will be determined by the junction numbers. Although some of the individual molecules of the type donor-spacer-acceptor between two electrodes would behave as molecular rectifiers under an electrical voltage bias, our current study promises potential applications of the atomic-scale p - n junctions operated on a macroscopic crystal. The ready operation on macroscopic crystals with microscopically electric features guides the future trend for new materials applications and fundamental study.

Conclusions

Our results have clearly presented for the first time the three oxidation states of manganese in perovskite oxides obtained by hydrothermal disproportionation reaction, and revealed the unique features of the atomic-scale p - n junctions based on the three valence states of manganese in the perovskite oxide. The atomic-scale p - n junctions of the single crystals naturally formed from hydrothermal systems may serve as a variety of electric devices for chip, memory, solar cell, and even water decomposition. In fact, the atomic-scale p - n junctions, beyond the nano-scale, provide potential applications of the atomic-scale electric devices operated through macroscopic crystals. Moreover, they may give rise to entirely new atomic-scale devices for applications to the atomic-effective processes on the photoelectric conversion [29] as well as the quantum information [30]. This study has experimentally revealed extraordinary phenomena of the three valence states of manganese. Further studies may open to other transition metal oxides and theoretical considerations as well.

Acknowledgements We thank Professors Martha Greenblatt, Kenneth Poeppelmeier, and Mark Ratner for helpful discussion. This work was supported by the National Nature Science Foundation of China (20631010 and 20121103) and the National High Technology Research and Development Program of China (863 Program) (No. 2006AA03Z410).

References

1. Bednorz JG, Mueller KA (1986) Z Phys B-Condensed Matter 64:189
2. von Helmlolt R, Wecker J, Holzapfel B, Schultz L, Samwer K (1993) Phys Rev Lett 71:2331

3. Tokura Y (2000) In: Sarma DD, Kotliar G, Tokura Y (eds) *Advances in condensed matter science*. vol. 2. Gordon and Breach Science Publishers, The Netherlands, pp 1–353
4. Renner Ch, Aeppli G, Kim B-G, Soh Y-Ah, Cheong S-W (2002) *Nature* 416:518
5. Millis AJ (1998) *Nature* 392:147
6. Rao CNR, Cheetham AK, Mahesh R (1996) *Chem Mater* 8:2421
7. Zener C (1951) *Phys Rev* 82:403
8. Schaak RE, Mallouk TE (2002) *Chem Mater* 14:1455
9. Woodward PM, Cox DE, Moshopoulou E, Sleight AW, Morimoto S (2000) *Phys Rev B* 62:844
10. Banach G, Temmerman WM (2004) *J Phys: Condens Matter* 16:S5633
11. Alonso JA, Martinez-Lope MJ, Casais MT, Garcia-Munoz JL, Fernandez-Diaz MT (2000) *Phys Rev B* 61:1756
12. Feng S, Xu R (2001) *Acc Chem Res* 34:239
13. Morale J, Sanchez L, Bach S, Pereira-Ramos JP (2002) *Mater Lett* 56:653
14. Feng S (1996) in *Proceedings of the 2nd International Conference on Solvo-thermal Reactions*, Takamatsu, (Org. Comm. Solvo-thermal Tech. Res. Ed. Japan, 1996) p. 118
15. Formula $\text{La}_{0.66}\text{Ca}_{0.29}\text{K}_{0.05}\text{MnO}_3$, space group $Pm\bar{3}m$, $a = 3.8864(4) \text{ \AA}$, $V = 58.701(10) \text{ \AA}^3$, $Z = 1$, $D_c = 5.890 \text{ g/cm}^3$, $\mu = 17.731 \text{ mm}^{-1}$, $F(000) = 93$, crystal size = $0.03 \times 0.03 \times 0.02 \text{ mm}^3$. Intensity data were collected on a Rigaku RAXIS-RAPID diffractometer (Mo-K α , graphite-monochromator) at a temperature of $293 \pm 2 \text{ K}$. The data processing was accomplished with the PROCESS-AUTO processing program. A total of 931 reflections ($5.25 < \theta < 27.22^\circ$) were collected, of which 26 unique reflections ($R_{\text{int}} = 0.0750$) were used. The structure was solved using the program SHELXS-97 and refined (5 parameters) using the program SHELXS-97 to R_1 ($I \geq 2\sigma(I)$) = 0.0381 and $wR_2 = 0.1052$. The La, Ca and K atoms occupied the same A-site. EXYZ and EADP were used to constrain the La/Ca/K ratio to 0.66/0.29/0.05 as measured by the ICP analysis. Further details of the crystal structure investigation may be obtained from the Fachinformationszentrum Karlsruhe, D-76344 Eggenstein-Leopoldshafen (Germany), on quoting the deposition number CSD 391346. The La, Ca and K atoms occupied the same A site.
16. Noginov MA, Loutts GB, Noginova N, Hurling S, Kück S (2000) *Phys Rev B* 61:1884
17. Bridges F, Booth CH, Anderson M, Kwei GH, Neumeier JJ, Snyder J, Mitchell J, Gardner JS, Brosha E (2001) *Phys Rev B* 63:214405
18. Reiche I, Vignaud C, Champagnon B, Panczer G, Brouder C, Morin G, Sole VA, Charlet L, Menu M (2001) *Am Mineralogist* 86:1519
19. Graft M, Reisfeld R, Panczer G (2005) *Modern luminescence spectroscopy of minerals and materials*. Springer-Berlin Heidelberg, New York, p 191
20. Shaker AM (2001) *Int J Chem Kinetics* 33:605
21. Jáky M, Simándi LI (1972) *J Chem Soc Perkin II*:1481
22. Deghoul F, Chermette H, Rogemond F, Moncorgé R, Stückl C, Daul C (1999) *Phy Rev B* 60:2404
23. Quarez E, Roussel P, Pérez O, Leligny H, Bendraoua A, Mentré O (2004) *Solid State Sci* 6:931
24. Otsuka Y, Naitoh Y, Matsumoto T, Kawai T (2003) *Appl Phys Lett* 82:1944
25. Wu Ch-G, Chang S-S (2005) *J Phys Chem B* 109:825
26. Ng M-K, Lee D-Ch, Yu L (2002) *J Am Chem Soc* 124:11862
27. Xu D, Watt GD, Harb JN, Davis RC (2005) *Nanoletters* 5:571
28. Aviram A, Ratner MA (1974) *Chem Phys Lett* 29:277
29. Kronik L, Shapira Y (1999) *Surf Sci Rep* 37:1
30. Kane BE (1998) *Nature* 393:133